Mikhal Ben-Joseph, Rivca Chaver, Michael Ho, Nagaprasad Rudrapatna, Emma Runia, Qi Xuan Khoo, Shine Wu

Turbulence: Prediction and Inference Through Statistical Modeling

I. Introduction

Our key **research objective was to gain a better understanding of the relationship between Froude number (Fr), Reynolds number (Re), and Stokes number (St) as predictors of turbulence**. We want to both understand and predict particle distribution and cloud formation, given data which describes the distribution of Voronoï volumes in terms of its first four raw moments. The raw moments of the distribution of Voronoï volumes were obtained via direct numerical simulation of turbulent flow for a given parameter space for Fr, Re, and St.

We designed two classes of models: one for inference and one for prediction. We evaluated our inferential model's success upon **interpretability as well as alignment to the physical interpretation** of these relationships. The predictive power of the inferential model was of interest but not the primary consideration during model selection. We assessed our predictive model's success strictly upon **minimization of cross-validation error** (according to the mean squared error criterion).

We conducted this research to help our engineering collaborators better understand how Fr, Re, and St influence various properties of the distribution of Voronoï volumes. In accordance with this objective, we assume that each of these constants are influential in the physical process of particle clustering. Additionally, we are given a fixed parameter range for each variable. However, we acknowledge that our engineering collaborators may wish to use our models to understand and/or predict the influence of Froude, Reynolds, and/or Stokes numbers beyond our training domains. Thus, since extrapolation beyond the training domains is likely of interest, we have calibrated our inferential and predictive models to accept a continuous range of values for each input.

II. Methodology

In fitting both classes of models, we opted to use the first four central moments of the distribution of Voronoï volumes as the response variables for our models, in order to enhance interpretability[1]. The inferential and predictive models are each composed of four submodels, one for each central moment (mean, variance, skewness, and kurtosis). We also applied an inverse logit transformation to the Froude number to convert our original range, [0, infinity), to a more useful interval, [0, 1]. Finally, we constructed categorical bins with cutoffs at each of the dataset's three unique values for the Froude number; the differences between the three values were so stark that we did not think it would be effective to try to extrapolate from them numerically. Because the Froude number has a critical value where flow shifts from subcritical to supercritical, creating ranges where we expect a certain type of flow is more interpretable. Having transformed the data, we then fit a simple linear model for each response.

Plots of the residuals as a function of fitted values for the simple linear models showed curvature, so we log-transformed the response variables in order to improve model fit. The probability distribution of Voronoï volumes is known to follow a log-normal distribution, and residual plots showed less curvature when log-transformed. Application of a Box-Cox transformation to test alternate transformations showed that a log-transformation of the response was optimal for each central moment.

[1] Formulas for our calculations of mean, variance, skewness, and kurtosis can be found in Appendix II: A

Plots of the log-transformed response variables as a function of Stokes number suggested a nonlinear relationship, so we compared the effects of quadratic and logarithmic transformations of the Stokes number on model fit. According to adjusted R-squared, AIC, and BIC, we found the logarithmic transformation to be optimal. We also considered using higher-order polynomials but decided it would make interpretation more difficult. Finally, we considered pairwise interaction effects between the Froude, Reynolds, and log-transformed Stokes numbers. We found that, for all responses, only including the interaction[2] between the log-transformed Reynolds number and the Froude number improved the model fit the most (i.e. lowest AIC and BIC).

After implementing the most effective transformations and adding the interaction term, we were still left with patterns in the residual plots for all four responses. We then decided to experiment with a semi-parametric modeling technique. Specifically, we created generalized additive models (GAMs) by partitioning the values of the Stokes number, fitting a model over each subinterval, and additively combining the models at each subinterval. GAMs were preferred to generalized linear models since combining the models at every subinterval allowed for greater flexibility to approximate local relationships, while preserving smoothness. We chose to place the two cutoffs (knots) at 0.4 and 0.9, the 33rd and 66th quantiles; additional knots provided marginal improvement in exchange for greater model complexity. However, this revealed an unresolved "fanning" effect in the residual plots. To address this, we log-transformed the Reynolds number. This transformation of Re improved model fit and corrected the "fanning" effect. Our proposed inferential models for all four log-transformed central moments are of the form[3],

$$\log(response) = \beta_0 + \beta_1 \times f_1(St) + \beta_2 \times f_2(St) + \beta_3 \times f_3(St) + \beta_4 \times \log(Re) + \beta_5 \times I(Fr_l) + \beta_6 \times I(Fr_m) + \beta_7 \times \log(Re) \times I(Fr_l) + \beta_8 \times \log(Re) \times I(Fr_m)$$

where f_1, f_2, and f_3 are components of the natural spline fit on the log-transformed Stokes number and each indicator function is either 0 or 1 depending on whether the Froude number is classified as low (l), medium (m), or high (h).

In our search for the optimal **predictive** model, we initially considered least-squares, penalized (ridge, lasso, elastic net), and k-nearest neighbors regression as well as the inferential model. However, after comparing the 10-fold **generalized cross-validation (mean-squared) errors** on subsets of the training data as a surrogate for the test data[4] between models, we determined that GAMs were the most promising technique for prediction. We examined the impact of each level-specific interaction effect on model accuracy. When modeling the log-transformed mean, we found that including any two of the three level-specific interaction terms produced the same level of accuracy; we chose to drop the interaction effect relating medium Froude number to log-transformed Reynolds number (i.e. $\log(Re) \times I(Fr_m)$) because medium Froude numbers accounted for the fewest number of test data observations. When

[2] We were motivated by figures, like Appendix A, to consider the interaction between log(Re) and Fr

[3] Inference coefficient estimates for each log-transformed central moment can be found in Appendix II: B-E

[4] We assumed that the test data does not include too much additional noise because it has the same parameter spaces for the Froude, Reynolds, and Stokes numbers, and the distribution of Voronoï volumes should not be drastically different in new experiments as the same physics applies.

modeling the other log-transformed central moments, we found that adding a fourth-order polynomial in Stokes number improved accuracy considerably. Including fifth or sixth-order terms only marginally improved accuracy, so we decided to omit them to reduce the risk of overfitting. After adding this term, only the interaction effect for the low Froude indicator decreased cross-validation error. Thus, we arrived at the following predictive model structures,

$\log(mean)$[5] =

$$\beta_0 + \beta_1 \times f_1(St) + \beta_2 \times f_2(St) + \beta_3 \times f_3(St) + \beta_4 \times \log(Re) + \beta_5 \times I(Fr_l) + \beta_6 \times I(Fr_m) + \beta_7 \times I(Fr_h) + \beta_8 \times \log(Re) \times I(Fr_l) + \beta_9 \times \log(Re) \times I(Fr_h)$$

$\log(response)$[6] =

$$\beta_0 + \beta_1 \times f_1(St) + \beta_2 \times f_2(St) + \beta_3 \times f_3(St) + \beta_4 \times \log(Re) + \beta_5 \times I(Fr_l) + \beta_6 \times I(Fr_m) + \beta_7 \times I(Fr_h) + \beta_8 \times St + \beta_9 \times St^2 + \beta_{10} \times St^3 + \beta_{11} \times St^4 + \beta_{12} \times \log(Re) \times I(Fr_l)$$

where f_1, f_2, and f_3 are components of the natural spline fit on the log-transformed Stokes number and each indicator function is either 0 or 1, as specified in the inferential model.

There are, however, a few limitations to our proposed inferential and predictive GAMs. For both the predictive and inferential models of the log-transformed mean (response), the residual plots displayed varying degrees of nonlinear patterns and highlighted some potential **outliers**. Furthermore, the QQ plots appeared nonlinear (deviates from a diagonal line). For both the predictive and inferential models of the other log-transformed central moments, the residual plots highlighted potential outliers and the QQ plots greatly deviated[7] from a diagonal line. Thus, although the predictive power of the model appears to be relatively high, the assumptions of an additive model are likely violated. These violations of the model assumptions may be explained by the presence of unusually large outliers. One strategy would be to remove these outlier points. However, since extrapolation beyond the training domain is a possibility, we were concerned that these outlier points may indeed appear normal given a larger training sample size. Since we decided to leave these points in the training data, our interpretations of the inferential GAM in the following section must be treated with caution.

III. Results

We observed consistent patterns across all submodels of the proposed inferential model. Firstly, the central moments each have a nonlinear relationship with the **Stokes number**. The change in the response variables was concave down as the Stokes number increased from 0 to approximately 0.3, ceteris paribus. Secondly, there was an inflection point at St = 0.4 where the responses, except for the mean, decreased as the Stokes number increased and another at St = 0.9 beyond which the increase in responses was approximately linear. The mean Voronoï volume did

[5] Prediction coefficient estimates for the log-transformed mean can be found in Appendix II: G

[6] Prediction coefficient estimates for log-transformed variance, skewness, and kurtosis can be found in Appendix II: H-J

[7] See Appendix L for an example of the nonlinear trend in the QQ plot

not decrease between 0.4 and 0.9, but the rate of change was almost flat[8]. From a physical perspective, this suggests that changes in particle size (Stokes number) are most impactful when the particle is very small, and that larger particles are associated with lower flow concentration. We expected this behavior since large particles, which often have irregular shapes, do not tessellate as easily as smaller particles.

The **Reynolds number** appears to have a negative linear relationship with the response in each of the four submodels of the proposed inferential model. For an increase in the Reynolds number, the expected Voronoï volume, variance, skewness, and kurtosis decrease on average, leading to increasingly concentrated particle clustering. This is consistent with existing literature showing that standard deviation decreases as Reynolds number increases for large Stokes numbers. Relative inertia may exert more influence on particle clustering for heavier particles, leading to less variability of Voronoï volumes.

Assuming ceteris paribus, a low **Froude number** (i.e. 0.052) corresponded to a higher value for expected Voronoï volume, variance, skewness, and kurtosis. However, when the Froude number is closer to 1, the effect is only statistically significant for the mean but not for the other responses in comparison with a high Froude number. Physically, this suggests that a low Froude number, which corresponds to subcritical flow—where small waves' upstream travel is possible— contributes to more tessellation; a high Froude number would correspond to lower tessellation.

Additionally, **the interaction effect between the Froude number and the log-transformed Reynolds number** has negative coefficient estimates in all submodels of the proposed inferential model. Specifically, when the Froude number is low, this interaction effect magnifies the negative effect of the Reynolds number on the responses compared to the baseline (high Froude number). This suggests that, when gravitational acceleration is lower, the effect of inertial force on particle clustering is more significant compared to when acceleration is higher. A Froude number close to 1 (i.e. 0.3) will also magnify the effect of the Reynolds number on expected Voronoï volume, though to a lesser extent. Such a Froude number does not appear to influence the effect of the Reynolds number on variance, skewness, and kurtosis.

To assess the performance of the predictive model, we produced a list of point predictions on the test set (in a .csv file) and evaluated the widths of the corresponding 95% prediction intervals for each point prediction. Based on Appendices M-P, these prediction intervals are not very wide relative to the mean values of each raw moment. However, we acknowledge that there are several sources of uncertainty in our predictions as a result of our model fitting procedure. Because we chose to incorporate the Froude number as a categorical variable based on flow type, we may be missing nuances of its effect on the responses. Additionally, though our use of natural splines creates better fit, it does impose less flexibility at the boundaries, causing more bias. Furthermore, given that there are much fewer data points in the training set for high Stokes numbers (only two unique data points for St >= 1 and St >= 2), prediction intervals for all four responses increase in width for higher Stokes numbers (as standard error increases).[9] With fewer data points at hand, the training model may potentially be overfitting the noise in the data set.

IV. Conclusion

[8] Plots of the effect of the Stokes number can be found in Appendix II: F

[9] This rationale is supported by Appendix G

There are several key takeaways from our analysis. Firstly, the influential predictors of the first four central moments (based on the inferential model) are: the Stokes number, the log-transformed Reynolds number, the Froude number, and the interaction between the log-transformed Reynolds number and the Froude number. Each predictor had a different effect: a low Stokes number is associated with higher flow concentration and vice versa, and incremental changes in the Stokes number are most impactful when it is low; the Reynolds number has a negative linear association with flow concentration; the Froude number indicates different types of flow, where a low Froude number is subcritical and associated with higher tessellation and a high Froude number is supercritical and associated with lower tessellation.

Notably, when the Froude number is low, the effect of the Reynolds number on the response variables is greater, suggesting that when flow is subcritical, a lower Reynolds number will result in more turbulence compared to when flow is supercritical. Additionally, while variance, skewness, and kurtosis are all affected by subcritical flow, there is no meaningful difference between how they are affected by supercritical flow and flow approaching critical. There is, however, a meaningful difference between how the mean is affected by supercritical flow and flow approaching critical.

Since these conclusions are inferences derived from analysis of the given dataset which contains discrete values of the predictors (except for Stokes number), further investigation is necessary to extrapolate the inferential and predictive models for a continuous parameter space of Fr, Re, and St.

V. Appendix I: References

Dou, Z., Bragg, A., Hammond, A., Liang, Z., Collins, L., & Meng, H. (2018). Effects of Reynolds number and Stokes number on particle-pair relative velocity in isotropic turbulence: A systematic experimental study. *Journal of Fluid Mechanics, 839*, 271-292. doi:10.1017/jfm.2017.813.

Thomas J. Overcamp & Steven E. Scarlett (1993) Effect of Reynolds Number on the Stokes Number of Cyclones, Aerosol Science and Technology, 19:3, 362-370, DOI: 10.1080/02786829308959643

Wang, X., Wan, M., Yang, Y., Wang, L.-P., & Chen, S. (2020). Reynolds number dependence of heavy particles clustering in homogeneous isotropic turbulence. *Physical Review Fluids*, *5*(12). DOI: 10.1103/physrevfluids.5.124603

VI. Appendix II: Supplementary Output and Figures

A. Visualizing the Relationship Between log(Re) and log(mean) by Fr

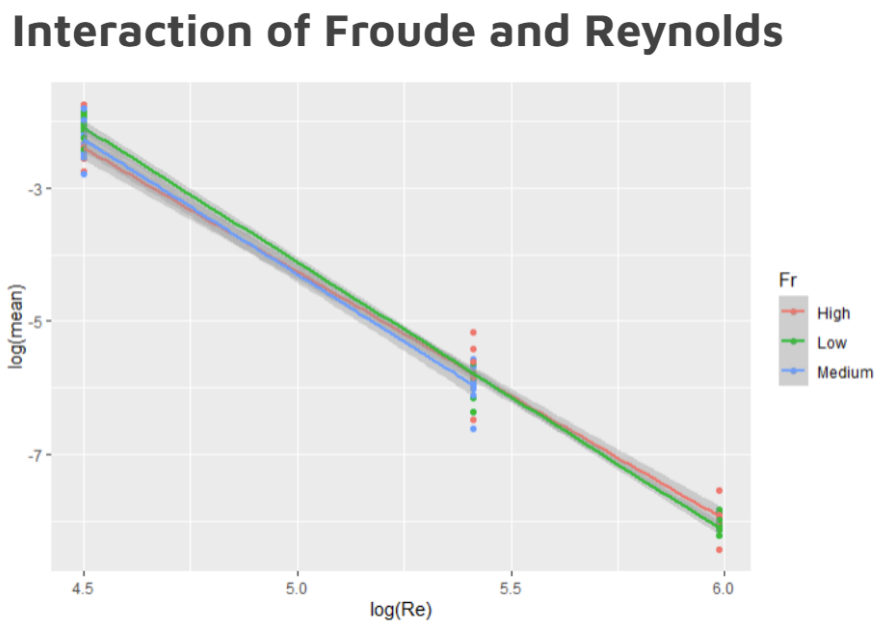

B. Conversion Formulas Between Raw and Central Moments

Mean = First Raw Moment
Variance = Second Raw Moment - Mean^2
Skewness = Third Raw Moment - 3 *(Mean * Second Raw Moment) + 2 * Mean^3
Kurtosis = Fourth Raw Moment - 4 * (Mean * Third Raw Moment) + 6 * (Second Raw Moment * Mean^2) - 3 * Mean^4

C. Coefficient Estimates (Inferential): log(Mean)

Coefficient	Estimate	Pr(>|t|)
(Intercept)	13.87537	<2e-16
ns(log(St), df = 3)1	0.34097	5.46e-13
ns(log(St), df = 3)2	1.17968	<2e-16
ns(log(St), df = 3)3	0.6918	<2e-16
log(Re)	-3.72089	<2e-16
FrLow	1.85764	1.03e-12
FrMedium	1.01626	0.000529
log(Re):FrLow	-0.3475	1.22e-12
log(Re):FrMedium	-0.21566	0.000175

D. Coefficient Estimates (Inferential): log(Variance)

Coefficient	Estimate	Pr(>|t|)
(Intercept)	9.7669	2.51e-12
ns(log(St), df = 3)1	2.0614	2.07e-10
ns(log(St), df = 3)2	8.7597	< 2e-16
ns(log(St), df = 3)3	2.2802	4.83e-13
log(Re)	-3.1214	< 2e-16
FrLow	28.0133	< 2e-16
FrMedium	0.4659	0.817
log(Re):FrLow	-4.7886	< 2e-16
log(Re):FrMedium	-0.1211	0.758

E. Coefficient Estimates (Inferential): log(Skewness)

Coefficient	Estimate	Pr(>|t|)
(Intercept)	8.84549	3.26e-05
ns(log(St), df = 3)1	3.06399	1.12e-08
ns(log(St), df = 3)2	13.63093	< 2e-16
ns(log(St), df = 3)3	3.19342	4.34e-10
log(Re)	-2.82005	5.85e-11
FrLow	53.14095	< 2e-16
FrMedium	0.16505	0.962
log(Re):FrLow	-9.03571	< 2e-16
log(Re):FrMedium	-0.08099	0.903

F. Coefficient Estimates (Inferential): log(Kurtosis)

Coefficient	Estimate	Pr(>|t|)
(Intercept)	8.64E+00	0.00236
ns(log(St), df = 3)1	3.92E+00	6.46e-08
ns(log(St), df = 3)2	1.79E+01	< 2e-16
ns(log(St), df = 3)3	3.99E+00	6.65e-09
log(Re)	-2.60E+00	2.39e-06
FrLow	7.79E+01	< 2e-16
FrMedium	5.96E-04	0.99990
log(Re):FrLow	-1.32E+01	< 2e-16
log(Re):FrMedium	-6.75E-02	0.94100

G. Plots of ns(log(St), df = 3)

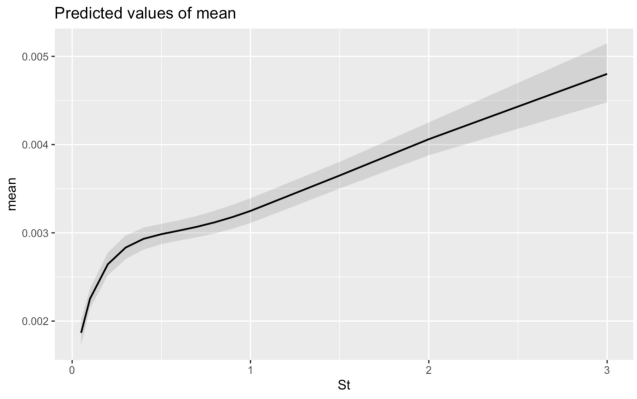

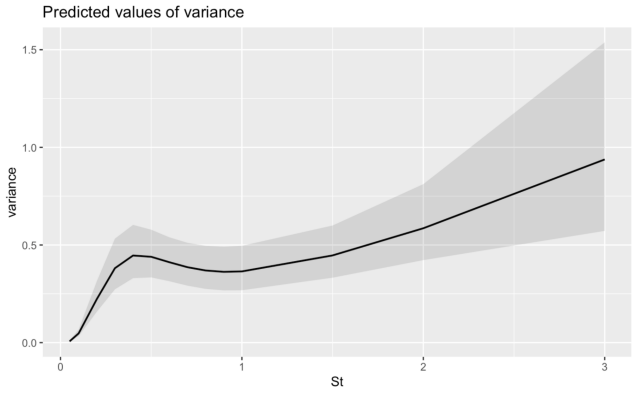

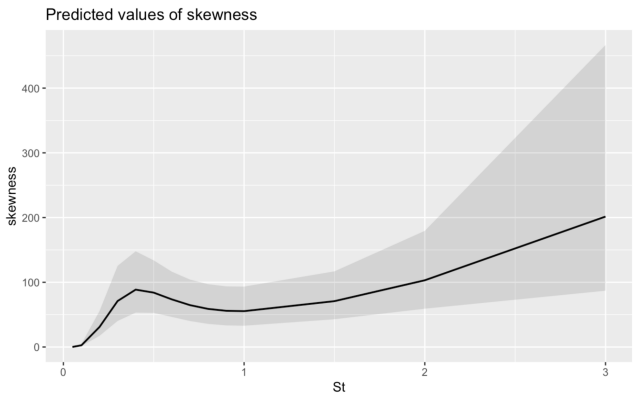

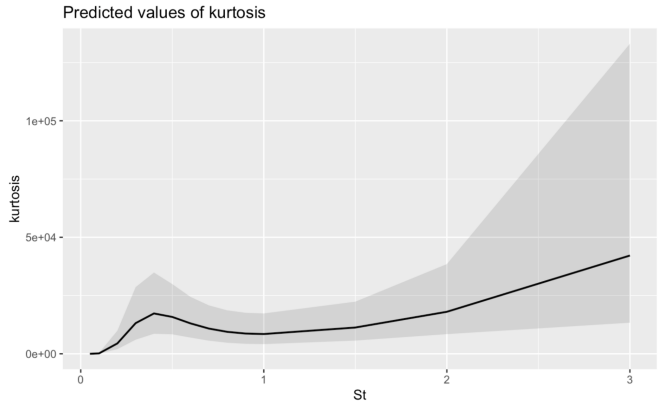

H. Coefficient Estimates (Predictive): log(Mean)

Coefficient	Estimate	Pr(>|t|)
(Intercept)	11.125	< 2e-16
ns(log(St), df = 3)1	0.34097	5.46E-13
ns(log(St), df = 3)2	1.17968	< 2e-16
ns(log(St), df = 3)3	0.6918	< 2e-16
log(Re)	-3.93655	< 2e-16
I(Fr == "Low")TRUE	4.608	< 2e-16
I(Fr == "Medium")TRUE	3.76663	< 2e-16
I(Fr == "High")TRUE	2.75037	< 2e-16
log(Re):I(Fr == "Low")TRUE	-0.13184	0.015435
log(Re):I(Fr == "High")TRUE	0.21566	0.000175

I. Coefficient Estimates (Predictive): log(Variance)

Coefficient	Estimate	Pr(>|t|)
(Intercept)	-110.465	0.074562
ns(log(St), df = 3)1	203.0738	0.035417
ns(log(St), df = 3)2	380.8339	0.047059
ns(log(St), df = 3)3	397.092	0.067141
log(Re)	-3.0649	< 2e-16
I(Fr == "Low")TRUE	-17.9182	0.381065
I(Fr == "Medium")TRUE	-46.3872	0.025831
I(Fr == "High")TRUE	-46.1597	0.02637
poly(St, 4)1	-1055.6763	0.068166
poly(St, 4)2	274.0644	0.020809
poly(St, 4)3	-65.3947	0.000659
poly(St, 4)4	9.6593	6.37E-06
log(Re):I(Fr == "Low")TRUE	-4.8457	< 2e-16

J. Coefficient Estimates (Predictive): log(Skewness)

Coefficient	Estimate	Pr(>|t|)
(Intercept)	-110.465	0.074562
ns(log(St), df = 3)1	203.0738	0.035417

ns(log(St), df = 3)2	380.8339	0.047059
ns(log(St), df = 3)3	397.092	0.067141
log(Re)	-3.0649	< 2e-16
I(Fr == "Low")TRUE	-17.9182	0.381065
I(Fr == "Medium")TRUE	-46.3872	0.025831
I(Fr == "High")TRUE	-46.1597	0.02637
poly(St, 4)1	-1055.6763	0.068166
poly(St, 4)2	274.0644	0.020809
poly(St, 4)3	-65.3947	0.000659
poly(St, 4)4	9.6593	6.37E-06
log(Re):I(Fr == "Low")TRUE	-4.8457	< 2e-16

K. Coefficient Estimates (Predictive): log(Kurtosis)

Coefficient	Estimate	Pr(>|t|)
(Intercept)	-260.5045	0.07495
ns(log(St), df = 3)1	464.7629	0.04131
ns(log(St), df = 3)2	872.1563	0.05395
ns(log(St), df = 3)3	912.2282	0.07475
log(Re)	-2.4033	2.26E-08
I(Fr == "Low")TRUE	-34.1577	0.47912
I(Fr == "Medium")TRUE	-113.4272	0.02116
I(Fr == "High")TRUE	-112.9196	0.02157
poly(St, 4)1	-2428.4026	0.07546
poly(St, 4)2	626.8417	0.02502
poly(St, 4)3	-147.9882	0.00106
poly(St, 4)4	21.4952	1.85E-05
log(Re):I(Fr == "Low")TRUE	-13.4112	< 2e-16

L. QQ Plot (Model in Appendix H)

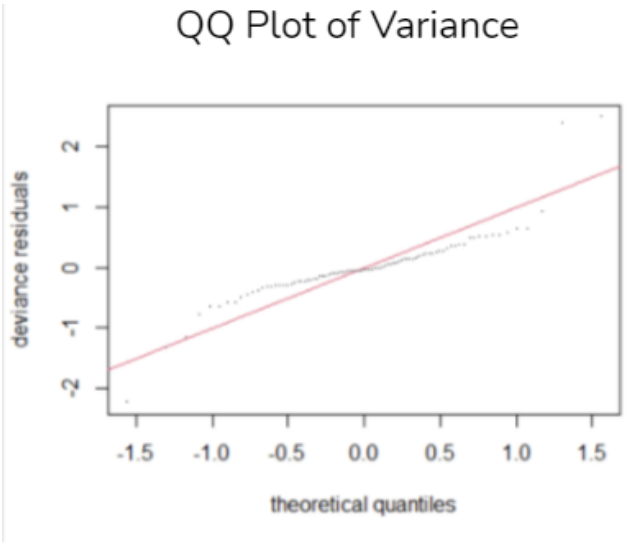

M. Prediction Estimates and 95% Prediction Intervals for the First Raw Moment Using Predictive Model

1	0.0001800553	0.0001967921	0.0001647420
2	0.0002550841	0.0002715868	0.0002395842
3	0.0002960474	0.0003130008	0.0002800123
4	0.0003133622	0.0003322841	0.0002955178
5	0.0002715889	0.0002901600	0.0002542064
6	0.0003646829	0.0003859954	0.0003445471
7	0.0003915182	0.0004161270	0.0003683647
8	0.0004399208	0.0004676761	0.0004138128
9	0.0005786727	0.0006307616	0.0005308854
10	0.0048011088	0.0051524984	0.0044736832
11	0.0023055634	0.0024255351	0.0021915258
12	0.0030540550	0.0031828370	0.0029304836
13	0.1197380954	0.1272366394	0.1126814694
14	0.1326682821	0.1409595077	0.1248647456
15	0.0762300944	0.0830051331	0.0700080474
16	0.1157202279	0.1233803399	0.1085356966
17	0.1235749810	0.1308664600	0.1166897609
18	0.1274071027	0.1352060620	0.1200580031
19	0.0892433561	0.0955572303	0.0833466666
20	0.0908595367	0.0970352672	0.0850768556

21	0.0921030688	0.0982958719	0.0863004225
22	0.1111049025	0.1187559892	0.1039467521
23	0.1236211533	0.1325671406	0.1152788654
1	0.0001800553	0.0001967921	0.0001647420

N. Prediction Estimates and 95% Prediction Intervals for the Second Raw Moment Using Predictive Model

	Estimate	Upper Bound	Lower Bound
1	3.857229e-05	7.065192e-05	2.106176e-05
2	2.755466e-03	4.646785e-03	1.633952e-03
3	4.038207e-03	5.935970e-03	2.747174e-03
4	3.993287e-03	5.992481e-03	2.661063e-03
5	2.749378e-03	5.025936e-03	1.504023e-03
6	8.743950e-03	1.283311e-02	5.957771e-03
7	8.597068e-03	1.277927e-02	5.783559e-03
8	1.436460e-02	2.530326e-02	8.154768e-03
9	1.784510e-02	3.282241e-02	9.702170e-03
10	7.820689e-01	1.323388e+00	4.621733e-01
11	1.601273e-02	2.766190e-02	9.269958e-03
12	4.711591e-02	6.755533e-02	3.286110e-02
13	4.133286e+02	6.544871e+02	2.610307e+02
14	5.113173e+02	7.725625e+02	3.384143e+02
15	4.940570e+00	8.842806e+00	2.760908e+00
16	3.845533e+02	5.977101e+02	2.474139e+02
17	5.200519e+02	7.791914e+02	3.470966e+02
18	4.991677e+02	7.438704e+02	3.349629e+02
19	6.698002e-01	1.084948e+00	4.141038e-01
20	7.787791e-01	1.235382e+00	4.915147e-01
21	8.412122e-01	1.287438e+00	5.501389e-01
22	1.380358e+00	2.432890e+00	7.845236e-01
23	1.332522e+00	2.383045e+00	7.468089e-01

O. Prediction Estimates and 95% Prediction Intervals for the Third Raw Moment Using Predictive Model

	Estimate	Upper Bound	Lower Bound

1	3.856069e-05	7.065489e-05	2.104502e-05
2	2.757510e-03	4.650497e-03	1.635069e-03
3	4.041706e-03	5.941446e-03	2.749403e-03
4	3.996943e-03	5.998344e-03	2.663335e-03
5	2.751544e-03	5.030227e-03	1.505106e-03
6	8.753383e-03	1.284782e-02	5.963810e-03
7	8.607013e-03	1.279505e-02	5.789814e-03
8	1.438336e-02	2.533854e-02	8.164720e-03
9	1.787574e-02	3.288412e-02	9.717340e-03
10	7.933100e-01	1.343817e+00	4.683559e-01
11	1.611814e-02	2.785727e-02	9.326081e-03
12	4.753821e-02	6.819019e-02	3.314136e-02
13	5.617844e+02	9.042911e+02	3.492551e+02
14	7.148018e+02	1.099237e+03	4.651628e+02
15	6.063734e+00	1.103677e+01	3.335178e+00
16	5.180386e+02	8.189281e+02	3.279592e+02
17	7.128291e+02	1.085080e+03	4.685877e+02
18	6.899399e+02	1.045575e+03	4.555900e+02
19	8.397399e-01	1.385096e+00	5.095416e-01
20	9.813020e-01	1.583765e+00	6.084946e-01
21	1.063601e+00	1.655527e+00	6.838374e-01
22	1.825364e+00	3.282198e+00	1.016118e+00
23	1.807645e+00	3.308552e+00	9.887296e-01

P. Prediction Estimates and 95% Prediction Intervals for the Fourth Raw Moment Using Predictive Model

	Estimate	Upper Bound	Lower Bound
1	8.079343e-05	3.375278e-04	1.934314e-05
2	6.812114e-01	2.340152e+00	1.982990e-01
3	1.212773e+00	3.012082e+00	4.883064e-01
4	1.014448e+00	2.645499e+00	3.890026e-01
5	7.257556e-01	3.016239e+00	1.746289e-01
6	5.922973e+00	1.465625e+01	2.393629e+00
7	4.653953e+00	1.186774e+01	1.825056e+00
8	1.184331e+01	4.509463e+01	3.110439e+00
9	1.504279e+01	6.343130e+01	3.567419e+00
10	2.907817e+04	1.007019e+05	8.396469e+03

11	2.889012e+00	1.050787e+01	7.943193e-01
12	2.070872e+01	4.850099e+01	8.842156e+00
13	1.363667e+10	4.037224e+10	4.606106e+09
14	1.646859e+10	4.364595e+10	6.213964e+09
15	1.311161e+06	5.188906e+06	3.313115e+05
16	1.219784e+10	3.456176e+10	4.304968e+09
17	2.095919e+10	5.445672e+10	8.066727e+09
18	1.726185e+10	4.428161e+10	6.729009e+09
19	1.375192e+02	4.327454e+02	4.373124e+01
20	1.856057e+02	5.553475e+02	6.206638e+01
21	2.113006e+02	5.804077e+02	7.695891e+01
22	4.225181e+02	1.621665e+03	1.101796e+02
23	3.470112e+02	1.381216e+03	8.728555e+01